EUROPEAN FUSION DEVELOPMENT AGREEMENT

EFDA–JET–CP(02)01/10

A. Huber, P. Coad, D. Coster, L.C. Ingesson, K. Itami, S. Jachmich,
A. Kirschner, M. Lehnen, G.F. Matthews, Ph. Mertens, V. Philipps,
A. Pospieszczyk, B. Schweer, G. Sergienko and M. Stamp

Tomographic Reconstruction of 2-D Line Radiation Distribution in the JET MkII GB Divertor

Tomographic Reconstruction of 2-D Line Radiation Distribution in the JET MkII GB Divertor

A. Huber[1], P. Coad[2], D. Coster[3], L.C. Ingesson[4], K Itami[5], S. Jachmich[1], A. Kirschner[1], M. Lehnen[1], G.F. Matthews[2], Ph. Mertens[1], V. Philipps[1], A. Pospieszczyk[1], B. Schweer[1], G. Sergienko[6], M. Stamp[2]
and contributors to the EFDA-JET workprogramme*

[1]Institut für Plasmaphysik, Forschungszentrum Jülich GmbH, EURATOM Association, Trilateral Euregio Cluster, D-52425 Jülich, Germany
[2]Euratom/UKAEA Fusion Association, Culham Science Centre, Abingdon, Oxon. OX14 3DB, UK
[3]Max-Planck-Institut für Plasmaphysik, Garching
[4]FOM-Instituut voor Plasmafysica, Nieuwegein, The Netherlands
[5]Japan Atomic Energy Research Institute, Naka-machi, Ibaraki-ken, Japan 311-0193
[6]Institute of High Temperatures, Russian Academy of Sciences, Moscow, Russian Federation
** See annex of J. Pamela et al, "Overview of Recent JET Results and Future Perspectives", Fusion Energy 2000 (Proc. 18th Int. Conf. Sorrento, 2000), IAEA, Vienna (2001).*

Preprint of Paper to be submitted for publication in
Proceedings of the 15th PSI Conference, (GIFU, Japan 22-31 May 2002)

ABSTRACT

A 2D-tomographic reconstruction of D_α– and C III emission distribution in L-mode density limit discharge has been performed using the Singular Value Decomposition method. Significant differences were observed in line emission between inner and outer divertor : at low central electron density ($\approx 2\times10^{19}$ m^{-3}), the maximum of the hydrogen radiation is located near the target plates at the position of the strike zone but with significantly more radiation from the inner leg than from the outer. The C III-radiation, on the other hand, is much stronger in the outer divertor, with a strong contribution near the X-point. With increasing density, D_α extends two-dimensionally within the inner divertor and, at the same time, the D_α radiation increases in the outer divertor. During the density rise, a reduction of C III-emission takes place, due to a decrease of the electron temperature and, accordingly, of the physical sputtering yield. It is shown that the major contributor to D_α emission, under the observed conditions, lies in excitation processes and that low-energy charge-exchange reactions with neutral deuterium can influence the ionisation balance of carbon and the recorded C III-emission line. Moreover, the emission patterns obtained from different diagnostics are in good agreement. The evolution of the intrinsic hydrogen and carbon impurity profiles in L-mode discharges is discussed with respect to its dependence on the location of methane fuelling.

1. INTRODUCTION

The amount and spatial distribution of impurity radiation in the divertor of a tokamak is of fundamental importance for the behaviour of power exhaust, detachment, recombination, recycling and erosion/redeposition properties. Carbon impurity radiation in the divertor is desirable to reduce the peak heat flux to the strike zones. But carbon erosion contributes also to MARFE formation, limits the lifetime of the target and leads to large tritium retention via co-deposition. In addition to line-integrated spectroscopic measurements, spatially resolved radiation of the various species obtained from tomographic inversion of 2D-CCD camera data is an important tool for diagnosing the role of impurity and hydrogen radiation in the divertor physics.

2. EXPERIMENTAL SETUP

At JET, three CCD cameras (KL1 diagnostic system, dynamical range of 8 bits, CCD-chip with 582×752 pixels) view the divertor in a nearly tangential geometry. They are coupled with interference filters and allow measurements of line-emission at three wavelengths (e.g. D_α, C II and C III simultaneously). Video signals are captured with a frame-grabber board, which transfers all images directly into the main memory. These cameras take video pictures at 50 half-frames per second. The evaluation of the 2D-emission distribution in a poloidal plane assumes toroidal symmetry and is obtained by solving the matrix equation Ax=b using the Singular Value Decomposition method [1]. Here, A is the "geometry matrix" that contains the information on the geometric view of each CCD-pixel and on the divertor structures limiting the corresponding lines of sight. The vector b contains the raw data (digitised CCD data). x is the unknown. As shown in [2], this camera system has enough

chords in the whole divertor region to resolve the emission pattern along the radial direction with sufficient resolution (<0.2 cm), but the resolution in z-direction (i.e. vertically) is limited to about 5 cm, owing to the small number of chords that actually cross each other at large angles.

The D_α distribution across inner and outer divertor is obtained with a spatial resolution of 3mm from the vertical view of an additional array camera (KL2). A survey spectrometer in the visible (KS3) provides integrated D_α and C III signals over both divertor legs. These two diagnostics are used for cross-calibration and for comparison with the reconstructed 2-D distributions of the line radiation.

3. RESULTS AND DISCUSSION

L-mode 'density limit' experiments have been performed with $B_T = 2.4$ T, $I_p = 2$ MA and with an additional NBI power of 2.3 MW. Figure 1 shows the time evolution of a typical L-mode density limit discharge in JET with the MkII GB divertor. The plasma density was raised steadily to the density limit by gas fuelling at constant input power. The integral ion flux to the outer divertor, measured by an array of Langmuir probes, initially increases, while the flux to the inner divertor remains at a constant level. This indicates that the inner divertor is partially detached from the start. At 17s, the integral ion flux to the inner divertor begins to fall as the density increases; it reaches a very low value around 20s. The D_α emission in the inner divertor (see Fig.3) and neutral pressure in the divertor chamber (not shown) continue to increase though. This is the signature of plasma detachment [3], which is characterised by a substantial drop both in particle and energy fluxes to the target plates, as well as in the pressure along the magnetic field lines. Shortly before the discharge disrupts, the ion flux to the outer divertor drops dramatically: a MARFE forms, which leads to a 'density limit' disruption. During the density increase time, the total radiated power is always increasing too. Figure 2 shows the tomographic reconstruction of D_α– (top) and C III-emission (bottom) in the divertor region at four different points in time:

- **Time 16.5s**: In this early phase of the discharge, the maximum of the hydrogen radiation is located near the target plates at the position of the strike zone but with significantly more radiation from the inner leg than from the outer. The electron temperature near the inner and outer strike points is about 8 eV and 18 eV, respectively. The C III-radiation is much stronger in the outer divertor, with an additional significant contribution near the X-point.
- **Time 17.5s**: The D_α–emission rapidly increases in the inner divertor. The ion flux to the inner divertor decreases, which indicates the start of the detachment. The Langmuir probes measure values of $T_e \approx$3-4 eV and $n_e = 2\times10^{19}$ m^{-3}, which, however, overestimates Te, since the standard interpretation of the I-V characteristic does not apply in this regime [4]. A small decrease (about 20%) in the C III-emission is observed in the outer divertor leg ($T_e \approx$13eV).
- **Time 19.5s**: While the D_α–emission extends in two dimensions in the inner divertor, the D_α–emission increases linearly with central average electron density and extends along the outer leg (near the outer strike point, $T_e \approx$6-7 eV). The spatial distribution of hydrogen radiation

is, in this discharge phase, more symmetrical. The ion flux at the outer strike point also increases. A strong reduction of C III-emission in the outer leg is observed.

– **Time 20.26**s: A drastic change in the D_α-emission happens together with full detachment of the inner divertor. The emission takes off from the inner target and moves to the X-point. The C III-emission is positioned above the X-point, a MARFE forms and moves towards the inner wall, which leads to a density-limit disruption.

The KS3 visible survey spectrometer provides integrated D_α and C III signals over inner and outer divertors, that are used for cross-calibration and for comparison with reconstructed 2-D distributions of line radiation. Figure 3. shows the time evolution of D_α (top) and C III (bottom) integrated emission both in inner and outer divertor. The solid lines shows the data from the spectrometer, and the symbols correspond to the simulation from tomographic reconstruction. For this simulation, D_α and C III reconstructed emissions were integrated along the same chord and averaged over the same radial extent as of the spectrometer. One sees that the simulated integrated emissions match the measured ones well during the whole discharge (lower than 10% for D_α and 20% for C III, respectively).

The reconstructed D_α-emission profiles have also been compared with the line-integrated emission of the D_α-hydrogen line, measured vertically from the top of the machine by an absolutely calibrated CCD camera array. As can be seen in Fig.4, the reconstructed poloidal D_α-emission profiles for two different times match the data from the camera array very well.

These profiles show results similar to those presented in fig.2. At the time point 16.5s, the profile shows a strong in-out asymmetry with significantly more radiation from the inner leg. As the density increases, the hydrogen emission increases in inner and outer divertor. An increase of intensity above the divertor septum is observed too. It should be also mentioned that the comparison between SVD (presented here) and Non-Negativity Constraint (used for radiation tomography) [5] shows a good agreement. As shown above, the D_α - and C III-emissions show a definite in-out asymmetry, depending on local plasma parameters. How can this asymmetry be explained? As Te at the inner strike point drops from 8eV to values below 3-4eV (again overestimated from the Langmuir probe), D_α increases by a factor of 3.5-4. The ratio of ionisation per photon for D_α , the so-called S/XB-value, decreases by a factor of 2 (from 25 (T_e = 8eV) to 12 (T_e = 4eV)), thereby indicating an actual increase of a factor of 2 (and not a factor of 4) for the D_α-emission, due to excitation only. The increase of a factor 4 in the hydrogen emission – for excitation only – can be explained if the temperature drops to a value of about 2eV. The influence of recombination on hydrogen emission shows Fig.5. Here, the D_α-emission rates corresponding to excitation and recombination for an electron density of $n_e = 2\times10^{19}$ m^{-3} are fetched from the ADAS data structure [6]. The emission rate for excitation is calculated for three different values of the neutral density n_0. The absolute D_α-emission due to recombination depends on n_e^2 , whereas the emission due to excitation depends on the product $n_e n_0$. Thus, the ratio of the emission from recombination to excitation depends on the

ratio n_e/n_0. One sees that the recombination becomes dominant for electron temperatures below 1.5eV, for any reasonable neutral density. The influence of recombination on the ratio D_γ/D_α is discussed in detail in [7]. If it is assumed that whole the radiation is caused by recombination, the ratio D_γ/D_α must lie around 0.15-0.2 for $n_e = 2\times10^{19}$ m^{-3} in the electronic temperature range T_e = 0.5-4eV. If all radiation is due to excitation, the ratio D_γ/D_α must be below 0.018. The measured ratio at t = 17.5s is about 0.03, confirming that the major contributing process to the D_α-emission is excitation.

Around 1.3eV, the ionisation and recombination rate coefficients are approximately equal [8]. For this temperature, the recombination rate coefficient is relatively low ($\leq10^{-17}$ m^3 s^{-1}), so that for $n_e = 2\times10^{19}$ m^{-3}, $\tau_{rec} \geq 5$ms. This characteristic time is comparable to or longer than the ion transit time in the divertor for a flow speed of ~10^3m/s. There is thus no sufficient time for volume recombination to occur.

As shown above, the C III radiation is much stronger in the outer divertor with the maximum at T_e = 13eV. Figure 5(b) shows effective emission rates for excitation Q_{exc} and recombination Q_{rec} for $n_e = 10^{19}$ m^{-3} as function of the electron temperature. By "effective emission rates" we mean the product of a photon emissivity coefficient (PEC) times the fractional abundance of carbon ions $f(^{Z+}) = n(C^{Z+})/n(C))$, where n(C) and $n(C^{Z+})$ is the total carbon density and the density of carbon ions with nuclear charge Z: $Q_{exc} = PEC_{exc} \times f(C^{2+})$, $Q_{rec} = PEC_{rec} \times f(C^{3+})$, $Q_{chs} = PEC_{chs} \times f(C^{3+})$, where Q_{chs} is an effective emission rate for charge exchange with neutral hydrogen. The intensity of the observed line (C III, λ = 465 nm) can be written $I= n_e \times n(C)[Q_{exc}+ Q_{rec}+ Q_{chs}]$. The PECs and fractional abundances were again calculated with the help of the ADAS structure and data base. The maximum in the calculated intensity per C atom lies around 5eV. Therefore, ionisation and recombination processes alone cannot explain the observed C III emission. Figure 5(c). shows values of Q which take into account the charge exchange processes with neutral hydrogen (deuterium) at a density of $n_d = 0.1 \times n_e$. The direct charge-exchange contribution to the line emission is negligible compared to electron-impact excitation. But it nevertheless shifts the ionisation balance to less ionised charge state distributions. The maximum of calculated line intensity per electron and carbon atom is shifted to higher electron temperatures and is located at 15eV. For small values of T_e, the line intensiy drops sharply (it is more than one order of magnitude smaller for T_e = 3-4eV, compared with T_e = 15eV), as seen in the experimental data. Thus, the strong in-out asymmetry in C III-emission can be explained by strong in-out asymmetry in T_e. For T_e = 13 eV, the charge-exchange rate coefficient (C^{3+} with D) is relatively large ($\geq2\times10^{-15}$ m^3 s^{-1}) [9], so that for $n_e = 2\times10^{19}$ $m^{-3} = 10\times n_0$, τ_{cxs} 0.25ms, i.e. much smaller than the ion transit time in the divertor for a flow speed of ~10^3 m/s. Thus, charge-exchange processes can sufficiently influence the C III emission.

Another possible reason for asymmetrical C III-emission would be a strong asymmetry in carbon erosion fluxes in inner and outer legs: in the outer divertor, the physical sputtering of C due to the impact of D and C dominates, whereas in the inner divertor, the chemical erosion of carbon due to molecule formation can lead to strong erosion even for hydrogen impact energies below the threshold

for physical sputtering (cf [10], where spectroscopic clues for such a behaviour are discussed in detail for O II and the very same line of C III as recorded in the present work). In order to study the influence of the impurity sources on line emission, a gas puffing experiment was performed. About 5×10^{21} CD_4 molecules per second were injected during L-mode discharges at different times into the inner and outer divertors, through a nozzle in the horizontal target plate (puff within the private flux zone). The magnetic configuration and plasma parameters were similar to the discharge shown in Fig.1 at t = 57.5s with strong in-out asymmetry: D_α radiates strongly in the inner leg, C III in the outer divertor. During the CD_4 injection into the outer divertor, the D_α emission shows a small increase in the outer leg (about 30%), but it is still much smaller than the emission from the inner divertor (S/XB(D_α) at outer strike point is relatively large, about 25). C III emission increases by about a factor of 2 in the vicinity of the gas puffing. The injection of CD_4 into the inner leg leads to a strong increase in D_α emission (about a factor of 3-4), but to practically no change in the C III emission in the inner divertor. Thus, the observed line emission in the divertor is strongly dependent on the local electron temperature.

4. SUMMARY AND CONCLUSION

2D emission profiles of C III and D_α radiation in the JET Divertor have been reconstructed by the Singular Value Decomposition method to obtain the emission pattern in a poloidal plane. In this contribution, the 2D-reconstructions of D_α - and C III-emissions in L-mode density limit discharges have been presented and analysed. Significant differences in line emission was observed between inner and outer divertor. At low central electron density ($\approx2\times10^{19}$ m^{-3}), the maximum of the hydrogen radiation is located near the target plates at the position of the strike zone, but with significantly more radiation from the inner leg than from the outer. The C III-radiation is much stronger in the outer divertor, with a strong contribution near the X-point as well. With increasing density, D_α extends two-dimensionally within the inner divertor and, at the same time, it goes up in the outer divertor. The D_α -emission is, at that time, nearly symmetrical. During the density rise, a reduction in C III-emission is observed, which corresponds to a decrease of the electron temperature and of the physical sputtering yield.

It has been shown that the major contributors to D_α -emission are, for the observed conditions, excitation processes and that low-energy charge-exchange reactions with neutral deuterium can influence the ionisation balance and the behaviour of the observed C III-emission line.

A good agreement between the emission pattern obtained from the different diagnostics is achieved. Moreover, the comparison between SVD and Non-Negativity Constraint Method shows a good correlation.

The evolution of the intrinsic hydrogen and carbon impurity profiles in L-mode discharges has been discussed, with respect to its dependence on the location of methane fuelling (inner/outer divertor leg). Interestingly, the C III-radiation of the carbon impurity fuelled via CD_4 injection in the divertor region shows a very similar pattern to that observed from intrinsic sources alone.

REFERENCES

[1]. G.H. Golub and C.F. Van Loan, John Hopkins University Press, Baltimore (1983).

[2]. A. Huber, P. Coad, D. Coster et al., in: Proceedings of the 28 th EPS Conference on Controlled Fusion and Plasma Physics, vol. **25A**, Funchal, Portugal, ECA (2001) p. 1649.

[3]. A. Loarte et al., Nucl. Fusion **38**, (1998) 331.

[4]. R. D. Monk et al., Contrib. Plasma Phys. **36**, (1996) 37.

[5]. L.C. Ingesson et al., Nucl. Fusion **38**, (1998) 1675.

[6]. H.P. Summers, *Atomic Data and Analysis Structure – User's Manual*, Rep. IR(94) 06, JET Joint Undertaking, Abingdon (1994) and http://adas.phys.strath.ac.uk

[7]. G.M. McCracken et al., Nucl. Fusion **38**, (1998) 619.

[8]. D.E. Post, J. Nucl. Mater. **220-222** (1995) 143.

[9]. C.F. Maggi et al, Plasma Phys. Control. Fusion **42** (2000) 669.

[10]. J.D. Hey et al., J. Phys. B: At. Mol. Opt. Phys. **35** (2002) 1525.

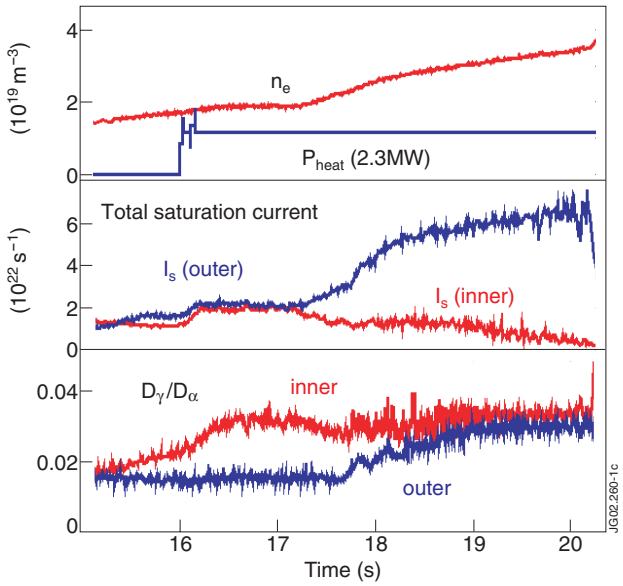

Figure 1: Time evolution of a typical L-mode, density limit discharge in JET with the MkIIGB divertor. The figure shows the central averaged density, the input power, the integrated ion flux to inner and outer divertors and D_γ/D_α emission line ratios at the inner and outer targets.

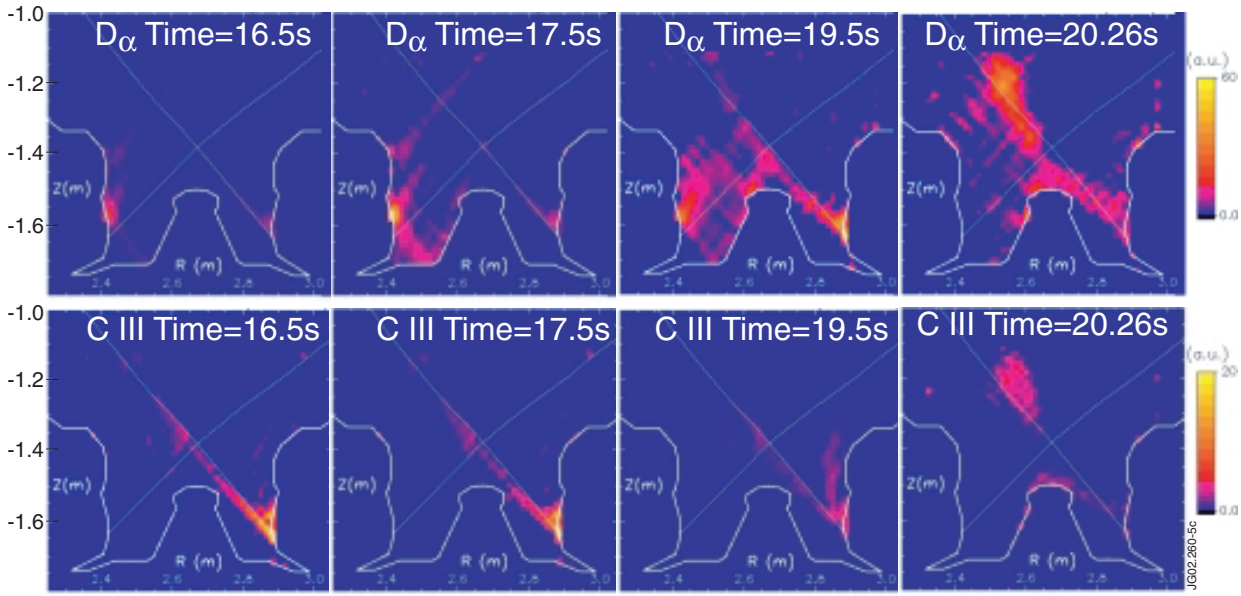

Figure 2: Tomographic reconstruction of D_α– (top) and C III-emission (bottom) in the divertor region measured by tangential CCD cameras during four phases of the L-mode density limit discharge.

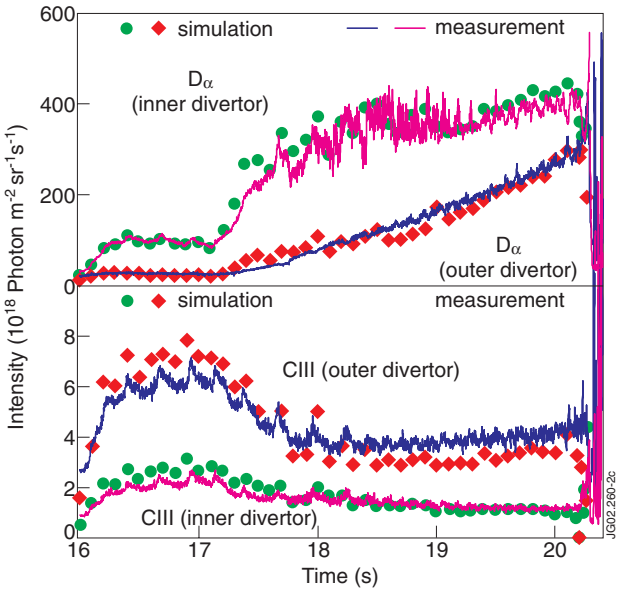

Figure 3: Time evolution of D_α (top) and C III (bottom) integrated emissions, shown with simulated data from a tomographic reconstruction.

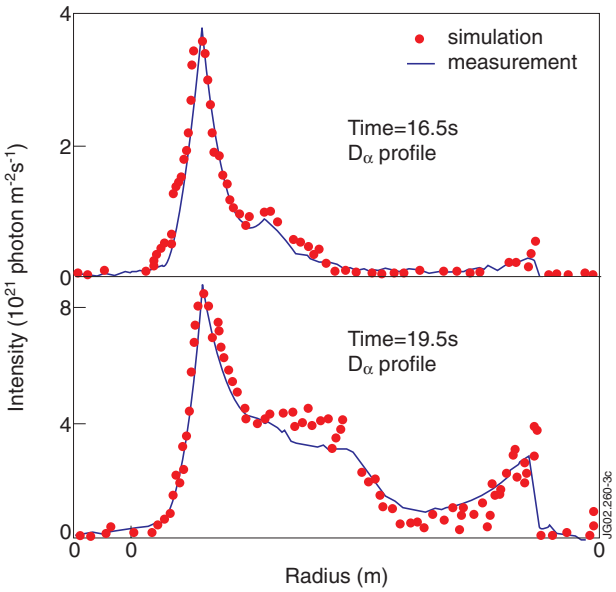

Figure 4: Comparison of reconstructed and measured (KL2) D_α– emission profiles.

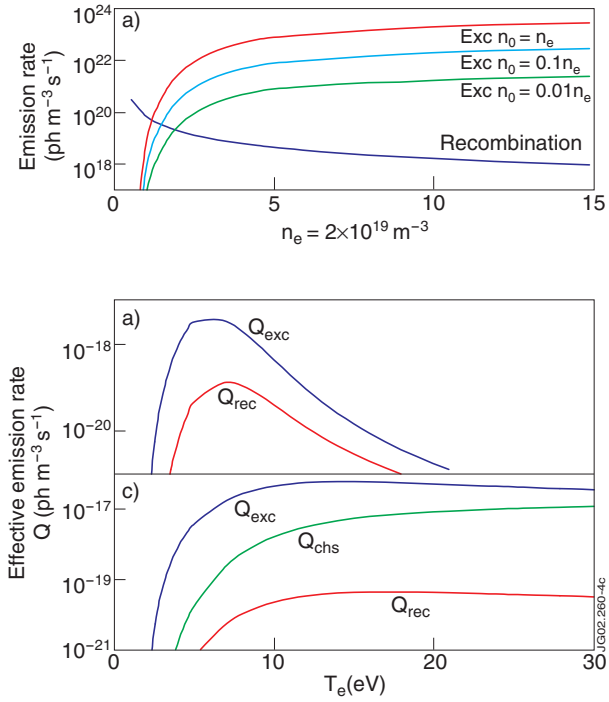

Figure 5: a) D_α–emission rates due to excitation (for three different neutral densities) and recombination for an electron density n_e=2×10^{19} m^{-3} from ADAS [6]; b) effective emission rates for excitation (Q_{exc}) and recombination (Q_{rec}); c) effective emission rates Q_{exc}, Q_{rec} and Q_{chs} (charge exchange), taking into account the charge-exchange processes with neutral deuterium for n_e=2×10^{19} m^{-3} and a neutral density of n_d=0.1×n_e.